JOURNAL OF NATURAL PRODUCTS

pubs.acs.org/jnp Article

Evaluation of Tandem Mass Spectrometry Experiments in the Negative Ionization Mode for Phenolamide Regioisomer Characterization

Irène Semay, Vincent Lemaur, Antoine Gekière, Maryse Vanderplanck, Pierre Duez, Denis Michez, and Pascal Gerbaux*

Cite This: https://doi.org/10.1021/acs.jnatprod.3c00047 Read Online

ACCESS | Metrics & More | Article Recommendations

ABSTRACT: Phenolamides are abundant specialized metabolites found in nature and consist of hydroxycinnamic acids mono- or polyconjugated with polyamines. Their participation in flower development is well-documented, and their presence in pollen raises the question of their role in pollen/pollinator interactions. The structural characterization of phenolamides is complicated by the presence of positional isomers and stereoisomers. Liquid chromatography coupled to tandem mass spectrometry in the positive ionization mode is becoming very popular in phenolamide structural characterization. However, collision-induced transamidation processes that cause the swapping of side chains have been detected, making it difficult to distinguish regioisomers with this technique. In the present report, we explore the dissociation processes undergone by the $[M - H]^-$ ions of spermidine-based phenolamides as model compounds. We describe two original competitive dissociation routes, namely, the phenolate and imidate pathways, to account for the observed fragmentation reactions undergone by collisional activated standard phenolamide anions. Whereas the phenolate pathway is regioselective at the central position for spermidine, the imidate pathway, requiring a deprotonated amide, only occurs at the extremities. Tandem mass spectrometry experiments on negatively charged phenolamide ions may then outperform their positive ionization mode counterparts for the distinction between phenolamide regioisomers and globally for the identification of phenolamides in natural extracts.

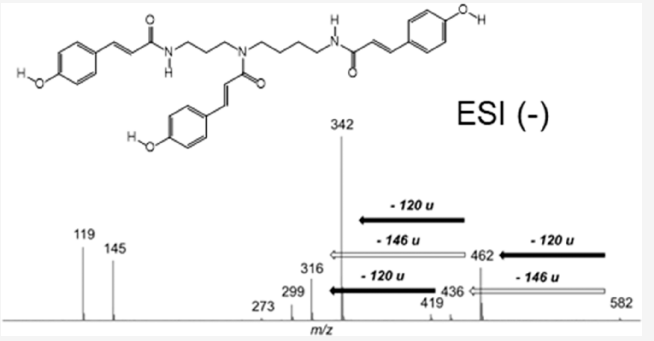

Phenolamides, also known as hydroxycinnamic acid amides (HCAAs), hydroxycinnamamides (HCA), or phenylamides, constitute one of the major classes of phenylpropanoids and consist of hydroxycinnamic acids mono- or polyconjugated with polyamines. These metabolites are evolutionarily conserved across angiosperms, including in Asteraceae (*Helianthus annuus* L.,[1] *Carthamus tinctorius* L.,[2] *Matricaria chamomilla* L.[3]), in Acanthaceae (*Aphelandra tetragona* Nees[4]), in Poaceae (*Zea mays* L.[5]), in Brassicaceae (*Arabidopsis thaliana* L.[6]), in Solanaceae (*Nicotiana attenuata* Torr.[7]), in Amaryllidaceae (*Hippeastrum* x hortorum[8]), and in Rosaceae (*Crataegus monogyna* Jacqu.[9]). They have been shown to play crucial biotic roles, in flower development, fertilization, senescence, and against pathogens, as well as abiotic roles in stress adaptation, UV protection, and oxidative stress resilience.[10] Phenolamides have also been detected[9] in the pollen of *C. monogyna* (common hawthorn; Rosaceae), their biological roles in the pollen coat are still debated (e.g., pollen−stigma recognition, pollen adhesion to pollinators[11]), and their potential impacts on pollinators remain poorly known.[12]

Phenolamides are composed of at least one hydroxycinnamic acid derivative linked through an amide bond to an aromatic monoamine or an aliphatic polyamine (Scheme 1). Whereas the most commonly linked hydroxycinnamic acids are *p*-coumaric, ferulic, caffeic, and sinapic acids, the aromatic monoamines are phenolic or indolic compounds, and the most common aliphatic polyamines are agmatine, putrescine, cadaverine, spermidine, and spermine,[13] The combination of all the different hydroxycinnamic acid and amine building blocks, together with the possibility of partial *N*-acylations of the aliphatic polyamines, generates immense structural diversity. In addition, due to the presence of the hydroxycinnamoyl chromophores, phenolamides have been abun-

Received: January 18, 2023

Scheme 1. Chemical Structures of Common Hydroxycinnamic Acids, Amines, and Phenolamides Found in Plants[a]

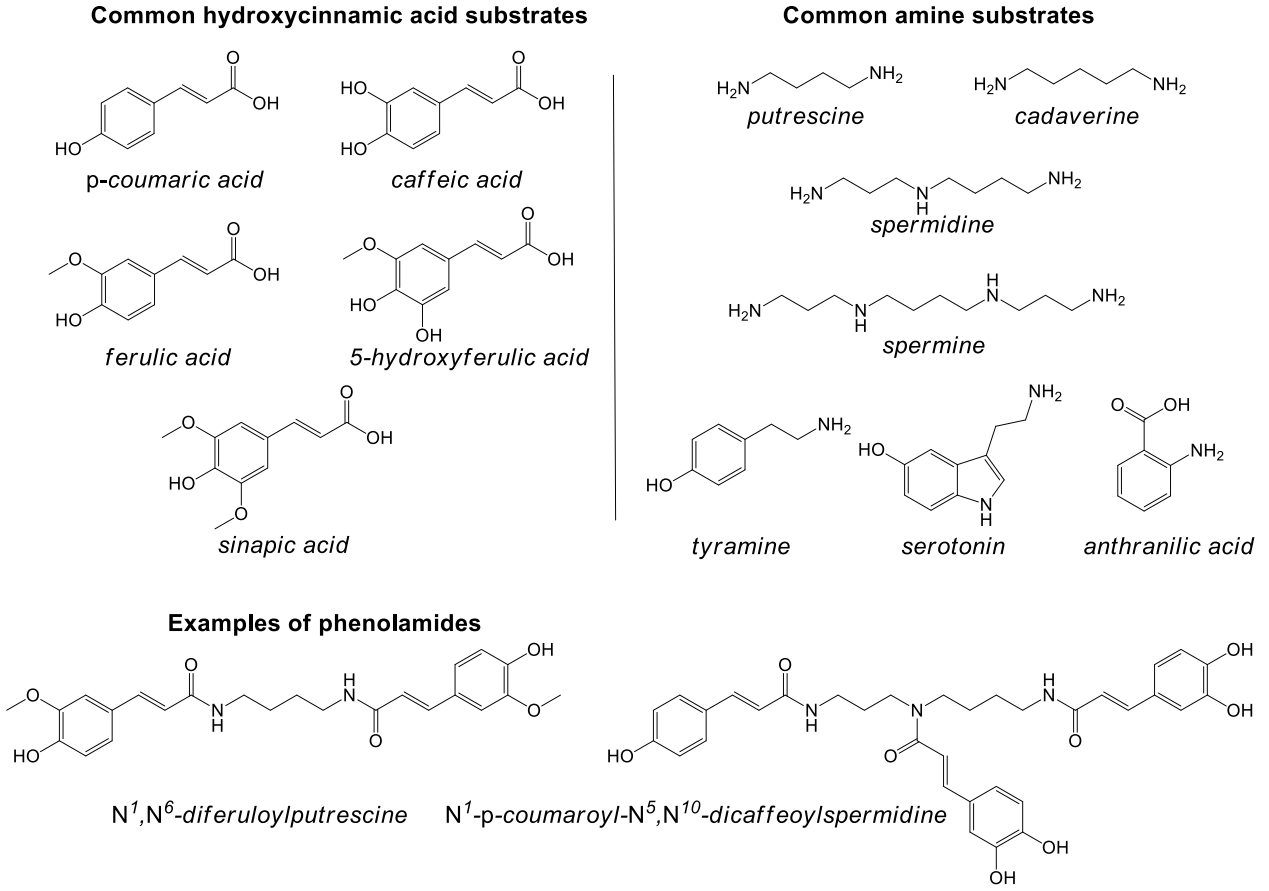

[a]Different degrees of substitution of the polyamine backbone are described with mono- or poly-substitution with the same or different hydroxycinnamic acids. All these combinations lead to a vast diversity of phenolamides.

dantly reported to undergo a *trans*-to-*cis* (or *E*-to-*Z*) isomerization under normal daylight conditions.[14] As for a typical example, the number of theoretically possible *cis*/*trans* and structural isomers is 12 for *N*,*N*′-dicoumaroylspermidines and 24 for *N*-coumaroyl-*N*′-feruloylspermidines.

Such an extreme diversity makes phenolamides challenging from a structural analysis point of view since, most of the time, the extracts contain a large number of congeners presenting only subtle structural differences, including different C=C configurations.[5] Mass spectrometry (MS), especially in combination with liquid chromatography (LC-MS), is widely used for phenolamide analysis.[6] Targeted[7] and untargeted[6,15] MS analyses based on liquid chromatography, high resolution measurements (exact mass measurements), and tandem mass spectrometry analyses are abundantly reported in the context of phenolamide biosynthesis investigations,[16] phenolamide regulation in front of insect attacks,[17] phenolamide chemical profiling in different plant extracts,[6] and phenolamide photoisomerization processes *in vivo* and *in vitro*.[8,18] Phenolamides, typically trisubstituted polyamines,[6,15] disubstituted spermidines,[19] or monosubstituted polyamines,[20,21] are most of the time analyzed using electrospray mass spectrometry (ESI-MS) in positive ionization mode by focusing on the $[M + H]^+$ ions. Collision-induced dissociation (CID) experiments on these $[M + H]^+$ ions have been discussed in the literature in the context of structural characterization,[6,15] and ion dissociation mechanisms have been proposed to explain the occurrence of the dominant fragment ions, namely, side-chain specific fragment ions. Unfortunately, transamidation reactions have been detected during the analysis by MS of di- and trisubstituted spermidines,[19] allowing the hydroxycinnamic groups to switch from one nitrogen atom to another on the polyamine backbone, precluding the distinction between regioisomeric phenolamides.

To the best of our knowledge, MS/MS analysis of phenolamides in the negative ionization mode is not documented in the literature. Therefore, in the present work, we decided to investigate the collision-induced dissociation (CID) behavior of $[M - H]^-$ ions on two types of derivatives: *(i)* synthetic spermidine-derived phenolamide standards, i.e., tricoumaroylspermidine, tricaffeoylspermidine, triferuloylspermidine, and dicaffeoylcoumaroylspermidine; and *(ii)* diamine-derivatives, i.e., diferuloylputrescine, diferuloyl-*N*-methylpropanediamine, and dicinnamoylcadaverine.

RESULTS AND DISCUSSION

N,*N*′,*N*′′-Tricoumaroylspermidine (**1**) (Scheme 2) was selected as the model phenolamide to initiate mechanistic investigations. Charge-directed reactions that are reported to be favored over charge-remote reactions under low-kinetic-energy CID were obviously considered for the phenolamide ion dissociation.[22]

To account for $[M + H]^+$ ion dissociation upon activation, the most comprehensive model is currently known as the "mobile proton" model.[23] A proton initially present at a basic

https://doi.org/10.1021/acs.jnatprod.3c00047
J. Nat. Prod. XXXX, XXX, XXX−XXX

Scheme 2. Deprotonation Sites Considered for Spermidine-Derived Phenolamides to Account for the Production of the [M − H]-Ion[a]

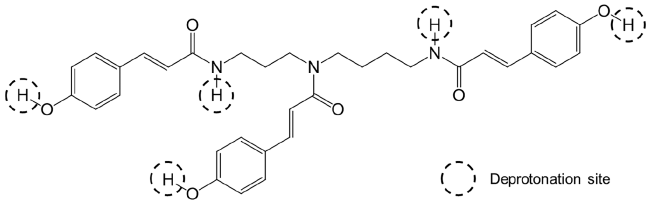

[a] *N,N′,N″*-Tricoumaroylspermidine (1) is represented.

site may endothermically migrate to a less basic functional group, generating fragile ions that promptly dissociate by eliminating a neutral moiety with low proton affinity. Regarding $[M - H]^-$ ions, the stable deprotonated molecules, i.e., deprotonated at the most acidic site, are proposed to undergo a proton migration (to the initially negatively charged atom) that repositions the negative charge to induce direct bond cleavages.[23] Obviously, for multifunctional analytes with multiple acidic and basic functional groups, the in-source production of quasi-isoenergetic protomers must also be considered to account for the occurrence of competitive dissociations. In Scheme 2, the acidic hydrogen atoms that are considered for the $[M - H]^-$ ion formation under ESI(−) conditions are identified.

Figure 1 presents the CID mass spectrum of the *m/z* 582 $[M\text{-}H]^-$ ions generated by the deprotonation of tricoumaroylspermidine (**1**) under ESI(−) ionization. As highlighted in the CID mass spectrum, the mass transitions dominantly correspond to 120 and 146 u losses that are associated with the coumaroyl moiety (147 u for the coumaroyl radical) yielding *m/z* 462 and 436 fragment ions, respectively. The detection of the complementary *m/z* 119 and 145 fragment ions suggests that the contribution of ion-neutral complex (INC) formation prior to the dissociation must be considered with or without charge retention at the initial deprotonation site,[24,25] making the [*m/z* 119/120 u loss] and [*m/z* 145/146 u loss] pairs intimately associated. When considering consecutive losses, it must also be noted that *(i)* the 146 u loss is unique (no consecutive 146 u losses), *(ii)* two consecutive 120 u losses can be detected but not three, and *(iii)* a 120 u loss may be consecutive to a 146 u loss (or *vice versa*).

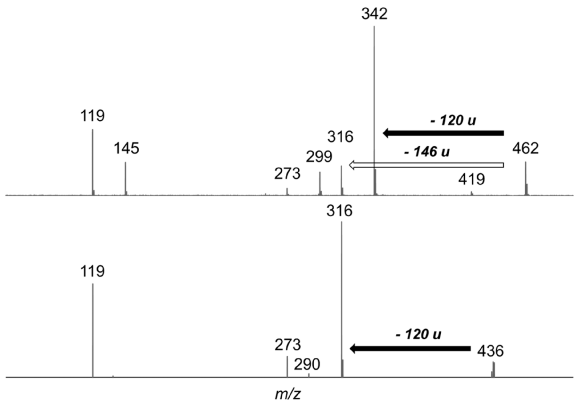

Figure 1. LC-MS/MS experiments: CID mass spectrum of the *m/z* 582 $[M - H]^-$ precursor ions corresponding to tricoumaroylspermidine (1) (Waters QToF API-US, ESI(−), collision energy (CE) = 30 eV). Black and white arrows, respectively, correspond to the imidate and phenolate pathways.

Based on the intrinsic acidities of the phenol ($pK_a \approx 10$) and amide ($pK_a \approx 17$) groups, we propose that the precursor ions are best considered as phenolate ions, i.e., with the negative charge being acquired upon phenol deprotonation. Of course, upon collisional activation, we may also hypothesize that proton migration between the terminal (N−H) amide functions and the phenolate may position the negative charge on one of the terminal amide functions (Scheme 2). We can then propose two distinct charge-driven mechanisms, depending on the position of the negative charge in the dissociating precursor ions. The first mechanism, named here the **phenolate pathway**, is presented in Scheme 3 and involves the dissociation of the N−C amide bond creating an ion-neutral complex that associates a deprotonated amine (here represented at the central position) and a neutral ketene (146 u). The dissociation of this complex may competitively afford the *m/z* 436 ions that are best represented as phenolate ions or the *m/z* 145 cumulene anions due to proton migrations between both partners within the ion-neutral complex. The phenolate mechanism is presented in Scheme 3 at the central position but must also be *a priori* considered at both extremities; however, as no consecutive 146 u losses are detected, this raises the question of the regiospecificity of this process (see below).

The second mechanism, i.e., **imidate pathway** (Scheme 4), involves a C−C bond dissociation generating another INC that associates a neutral isocyanate to a deprotonated alkene (*m/z* 119). Proton transfers between both partners within the INC prior to the dissociation will competitively afford, by a 120 u loss, the *m/z* 462 fragment ions, here represented as phenolate ions, or the *m/z* 119 ions, also presented as phenolate ions. The presence of the isocyanate moiety in the *m/z* 462 ions is confirmed by a further isocyanic acid (H−N═C═O) loss, leading to the *m/z* 419 fragment ions.

Regarding the *m/z* 436 and *m/z* 462 fragment ions, consecutive decompositions may occur by either the phenolate or imidate pathways. The *m/z* 436 ions, bearing both phenol and amide groups, may *a priori* undergo both decomposition reactions, but as shown in Figure 1, no additional 146 u loss (phenolate pathway) is detected, pointing again to the suggested "central" regioselectivity of this process. However, a 120 u loss is clearly observed, yielding the *m/z* 316 ions by the imidate pathway. From the *m/z* 462 ions, both the 120 and 146 u losses are detected in Figure 1, generating the *m/z* 342 and *m/z* 316 ions, respectively, through the imidate and the phenolate pathways. We confirm using pseudo-MS^3 experiments (Figure 2) that the *m/z* 316 ions are fragment ions of both the *m/z* 462 (146 u loss) and *m/z* 436 (120 u loss) ions (see Experimental Section for details).

Finally, because the *m/z* 316 ions still include a coumaroyl residue, a 120 u loss according to the imidate pathway could *a priori* be envisaged but is not observed due to the weaker acidity of the diisocyanate compared to the phenol, and only the *m/z* 119 phenolate ions are generated.

At this point of the study, the detection of the regiospecificity of the phenolate pathway at the central position and of the imidate pathway at both extremities of the spermidine derivatives suggests the possibility of discriminating the N^1/N^{10} positions from the N^5. The CID analysis in negative ion mode could then be efficiently used to identify the N^5 hydroxycinnamic acid residues.

https://doi.org/10.1021/acs.jnatprod.3c00047
J. Nat. Prod. XXXX, XXX, XXX−XXX

Scheme 3. CID Experiments on Deprotonated Phenolamides: Phenolate Pathway—146 u loss and *m/z* 145 Production—from Deprotonated Tricoumaroylspermidine (1)[a]

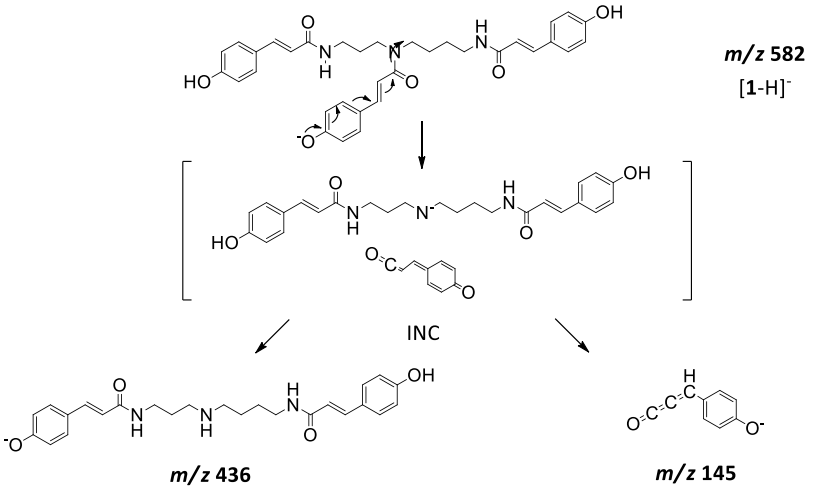

[a]Note that the dissociation of the ion-neutral complex (INC) may competitively produce *m/z* 145 and 436 fragment ions due to proton transfers prior to dissociation (see text).

Scheme 4. CID Experiments on Deprotonated Phenolamides: Imidate Pathway−120 u Loss−on Tricoumaroylspermidine (1)[a]

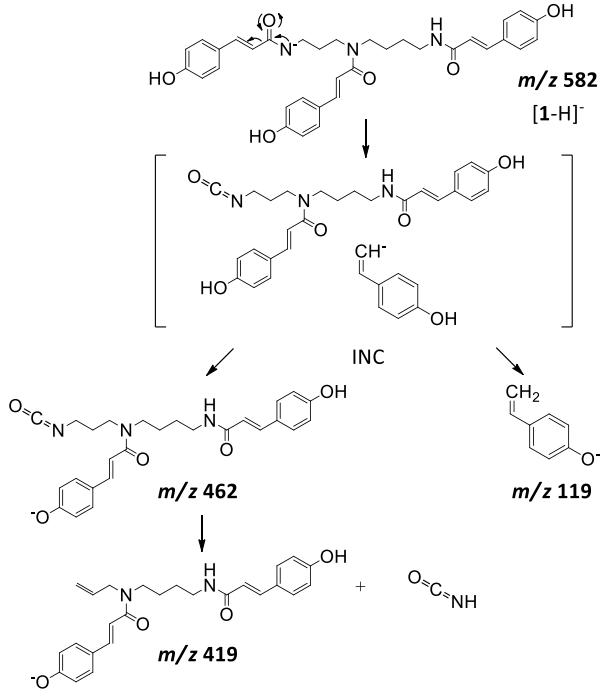

[a]Note that the dissociation of the ion-neutral complex (INC) may competitively produce *m/z* 119 and 462 fragment ions due to proton transfers prior to dissociation (see text).

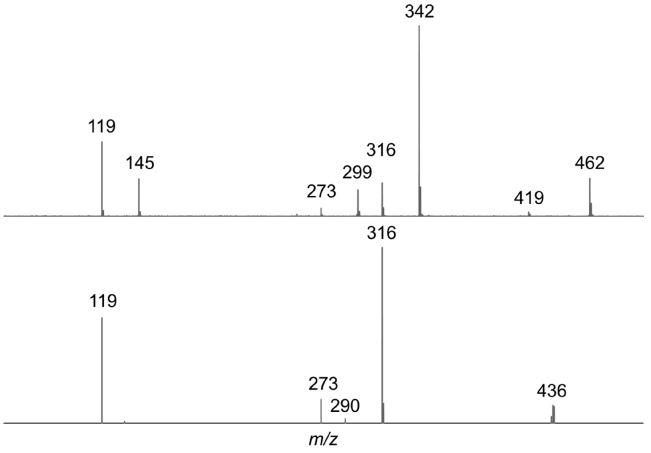

Figure 2. Pseudo-MS^3 experiments on the *m/z* 582 $[M - H]^-$ precursor ions corresponding to tricoumaroylspermidine (1). Top: CID spectrum of *m/z* 436 $[M - H]^-$, fragment ions of deprotonated (1) generated by the phenolate pathway. Bottom: CID spectrum of *m/z* 462 $[M - H]^-$, fragment ions of deprotonated (1) generated by the imidate pathway (Waters QToF API-US, ESI(−), cone voltage = 90 V, CE = 20 eV).

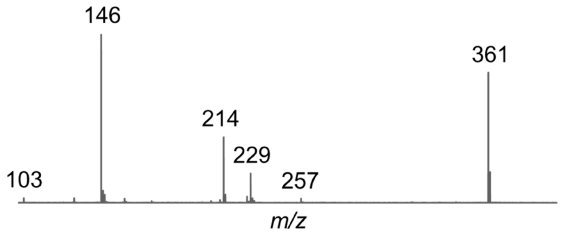

Figure 3. LC-MS/MS experiments: CID mass spectrum of the *m/z* 361 $[M - H]^-$ precursor ions corresponding to N^1,N^7-dicinnamoylcadaverine (2) (Waters QToF API-US, ESI(−), collision energy (CE) = 20 eV).

To reinforce the key role played by the phenol groups on the fragmentation pathways in negative ionization mode, we recorded the CID spectrum of deprotonated N^1,N^7-dicinnamoylcadaverine (**2**) ions (Figure 3 and Scheme 5).

As expected, fragment ions related to the phenolate decomposition pathway (*m/z* 129 and *m/z* 231) are not detected. Interestingly, the imidate pathway is also severely hampered by the absence of phenol groups, with the signals corresponding to the fragment ions *m/z* 103 and 257 being marginally detected. However, starting from the imidate precursor ions, i.e., deprotonated dicinnamoylcadaverine (**2**), we propose that a nucleophilic substitution produces the cinnamoyl residue as a conjugated imidate detected at *m/z*

https://doi.org/10.1021/acs.jnatprod.3c00047
J. Nat. Prod. XXXX, XXX, XXX−XXX

Scheme 5. CID Experiments on Deprotonated Phenolamides: Proposed Mechanism for the Formation of the *m/z* 146 Ions from Deprotonated N^1,N^7-Dicinnamoylcadaverine (2)

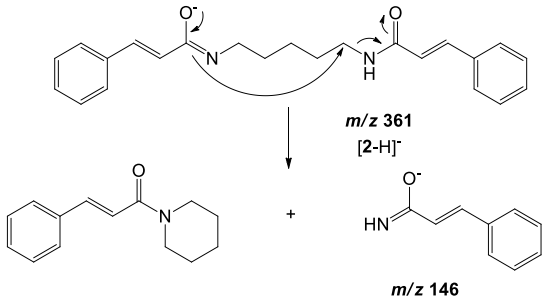

146. Note that the intermediacy of an INC is also suspected due to the presence of complementary *m/z* 214 ions. The production of a six-membered ring neutral fragment (Scheme 5) probably represents the driving force of this specific decomposition, revealing that modifying the number of methylene groups between both amides will certainly affect the decomposition reaction efficiencies.

Another useful example that could be envisaged is the differentiation between ferulic and isoferulic acid amides because switching the position of the phenol from para to meta is likely to eliminate the phenolate fragmentation pathway.

Methoxylated residues, namely, feruloyl, sinapoyl, and hydroxyferuloyl derivatives, are often encountered among the phenolamide family members; see Scheme 1. The CID mass spectrum of the $[M - H]^-$ ions of triferuloylspermidine (**3**) is presented in Figure 4 and features the fragment ions expected on the basis of the phenolate and imidate pathways.

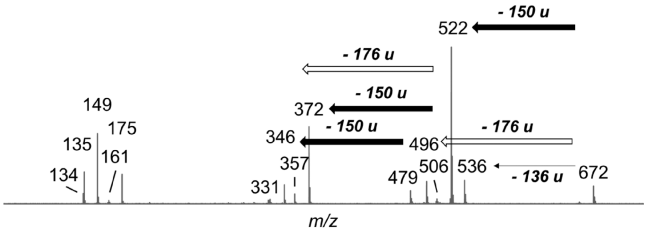

Figure 4. LC-MS/MS analysis of the triferuloylspermidine (**3**) standard. CID mass spectrum of *m/z* 672 $[M - H]^-$ ions (Waters QToF API-US, ESI(−), CE = 30 eV). Black and white arrows respectively correspond to the imidate and phenolate pathways. The thin arrow corresponds to the methyl migration + imidate pathway combination.

Indeed, the detection of the [*m/z* 149/150 u loss] and [*m/z* 175/176 u loss] definitely confirms the presence of the feruloyl residue. Again, the 43 u loss (HNCO loss) from the *m/z* 522 ions is clearly observed at *m/z* 479, confirming the presence of an isocyanate group in the fragment ions.

However, the observation of the *m/z* 536 ions, i.e., a 136 u loss typical of the caffeoyl group at N^1/N^{10}, must find its origin in another process. This 136 u loss is accompanied by the complementary production of the *m/z* 135 fragment ions. We propose that, for methoxylated substituents such as feruloyl, a CH_3 group (formally a CH_3^+) is transferred from a N^1 or N^{10} feruloyl residue to the deprotonated central feruloyl residue, see Scheme 6, creating a caffeoyl residue at N^1 or N^{10}. A

Scheme 6. CID Experiments on Deprotonated Phenolamides: The 136 u Loss from the $[M - H]^-$ Ions of Triferuloylspermidine (3) Involves a Methyl Cation Migration from a Feruloyl Side Chain to a Phenolate Group[a]

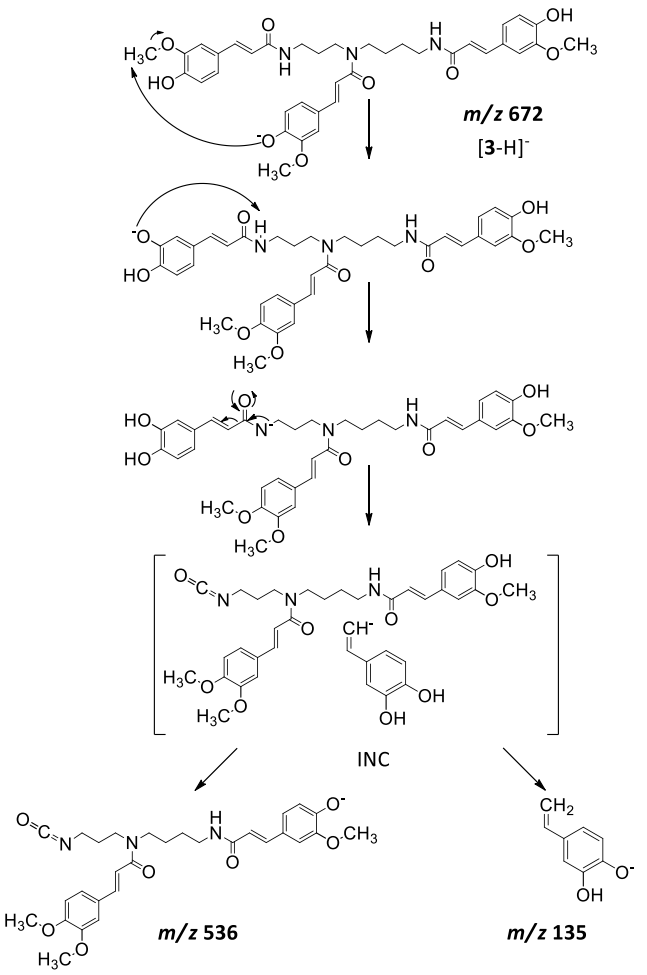

[a]This process mitigates the regioisomer distinction by interconverting a side chain into another. Note that the dissociation of the ion-neutral complex (INC) may competitively produce *m/z* 135 and 536 fragment ions due to proton transfers prior to dissociation (see text).

subsequent imidate pathway reaction then affords the *m/z* 536 ions (136 u loss) and the complementary *m/z* 135 ions, as depicted in Scheme 6. Such a "methyl migration" mechanism must be considered with great care for methoxy-containing hydroxycinnamic acid residues, since it complicates the interpretation of the spectra by interconverting the side chains into other hydroxycinnamic acid residues.

To further strengthen our mechanistic propositions, we prepared a diamine phenolamide, i.e., N^1,N^6-diferuloylputrescine (**4**) (Figure 5a). In this molecule, as no central hydroxycinnamic acid residue is present, the regioselectivity of the phenolate pathway and the "methyl migration" process can be tested. The imidate pathway clearly represents the dominant dissociation route with detection of abundant *m/z* 289 (150 unit loss) and *m/z* 149 ions. The phenolate pathway is opened although marginally observed at *m/z* 175 and *m/z* 263, allowing us to conclude that this pathway is selectively, but not specifically, occurring at the central position of the triamine phenolamide. The *m/z* 135 fragment ions can be

https://doi.org/10.1021/acs.jnatprod.3c00047
J. Nat. Prod. XXXX, XXX, XXX−XXX

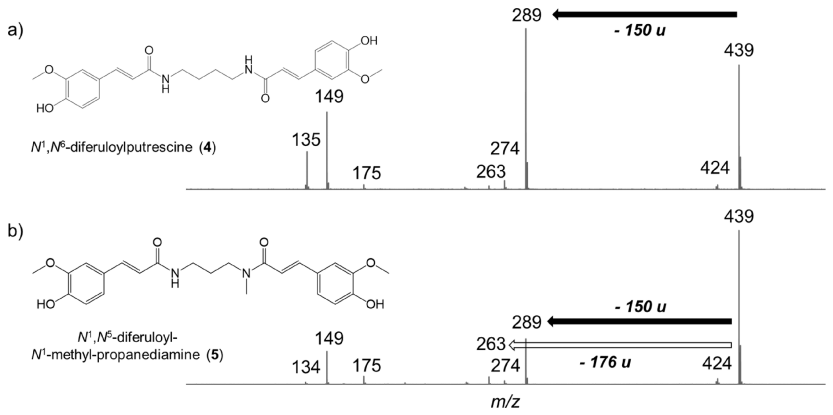

Figure 5. LC-MS/MS analysis of (a) N^1,N^6-diferuloylputrescine (**4**) and (b) N^1,N^5-diferuloyl-N^1-methylpropanediamine (**5**): CID mass spectra of the m/z 439 $[M - H]^-$ ions (Waters QToF API-US, ESI(−), CE = 15 eV). Black and white arrows respectively correspond to the imidate and phenolate pathways.

associated with a caffeoyl residue via the imidate pathway initiated by a "methyl migration" from one feruloyl residue to the other.

We finally prepared N^1,N^5-diferuloyl-N^1-methylpropanediamine (**5**) (Figure 5b), which is an isomer of **4** with the main differences being a shorter alkyl chain between both amines (three methylenes vs four methylenes) and a *N*,*N*-dialkylamide function in **5**, reminiscent of the central position in the triamines **1** and **3**. The shorter alkyl chain in **5** was selected because a methyl migration between both extremities would require a high conformational flexibility. Interestingly, the comparison between the CID spectra of **4** and **5** reveals that the "methyl migration" process seems less favorable in **5** with a by far weaker intensity of the m/z 135 ions. The m/z 134 ions are ascribed to a methyl radical loss from m/z 149.

Whereas the imidate pathway may only occur at the terminal pathway, the selectivity of the phenolate pathway at the central position, as observed in Figure 5, was less straightforward to understand, since such a pathway is likely to occur at both positions. The imidate/phenolate competition at the terminal position has thus been investigated by estimating the thermal enthalpies of the competitive reactions at the MP2/6-31G** level, as shown in Scheme 7. Note first that using *N*′,*N*′′-dimethylhydroxycinnamide as a central position model compound, we calculated that the thermal enthalpy of the phenolate pathway dissociation toward CH_3-N^--CH_3 ions amounts to 115 kcal/mol.

Scheme 7. Energy Diagram (MP2/6-31G Calculated Thermal Enthalpies) for the CID Decomposition of *N*-Ethylhydroxycinnamide Negative Ions: Phenolate vs Imidate Pathways for the Regioselectivity Analysis**

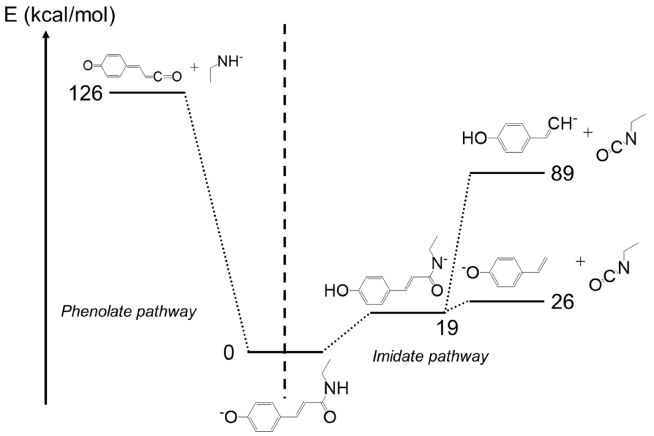

N-Ethylhydroxycinnamide was designed to mimic the terminal position of the spermidine phenolamides. Upon deprotonation under ESI(−) conditions, the phenolate pathway is occurring starting from the phenolate precursor ions and requires around 126 kcal/mol to occur, see Scheme 7. However, the imidate pathway, which is opened from the *N*-ethyl isomer after a slightly energetic proton transfer (19 kcal/mol) toward the imidate ions, only costs 89 kcal/mol to occur, yielding neutral isocyanate and C-deprotonated hydroxystyrene. The efficiency of this pathway is even more striking when considering that, before dissociation of the ion neutral complex (INC), a favorable proton transfer may generate O-deprotonated hydroxystyrene with a global thermal enthalpy of only 26 kcal/mol. These theoretical results thus reveal that the imidate pathway is by far less energy demanding at the terminal position than the phenolate pathway and that phenolate pathway is regioselective at the central position of spermidine phenolamides, as the more favorable imidate pathway is not possible at that position.

To further test the discrimination between the N^1/N^{10} positions and the N^5 one, the three positional isomers of dicaffeoylcoumaroylspermidine (**6**, **7**, and **8**) were tentatively prepared in a one-pot synthesis by introducing spermidine/caffeic acid/coumaric acid in a 1/2/1 molar ratio (see the Experimental Section). The three isomers **6**, **7** and **8** are only distinguished by the relative positions of the coumaroyl and caffeoyl residues, with the unique coumaroyl residue being anchored at N^5, N^{10}, and N^1, respectively. First of all, accurate mass measurements in ESI(+) confirmed the obtention of dicaffeoylcoumarylspermidine ($[M + H]^+$; $C_{34}H_{38}N_3O_8^+$; measured mass at m/z 616.2628; theoretical mass at m/z 616.2659; mass error 5.0 ppm). Upon LC-MS analysis in negative ionization mode, as presented in Figure 6, two signals, corresponding to the m/z 614 ions, were detected at 18 and 18.2 min, suggesting the presence of at least two regioisomers out of the three expected, whereas it is reasonable to assume that both **7** and **8** were both actually formed due to the quasi-symmetric triamine starting material (spermidine). Such a narrow time window, ∼10 s, also confirmed the analytical challenge for regioisomeric phenolamide characterization.

https://doi.org/10.1021/acs.jnatprod.3c00047
J. Nat. Prod. XXXX, XXX, XXX−XXX

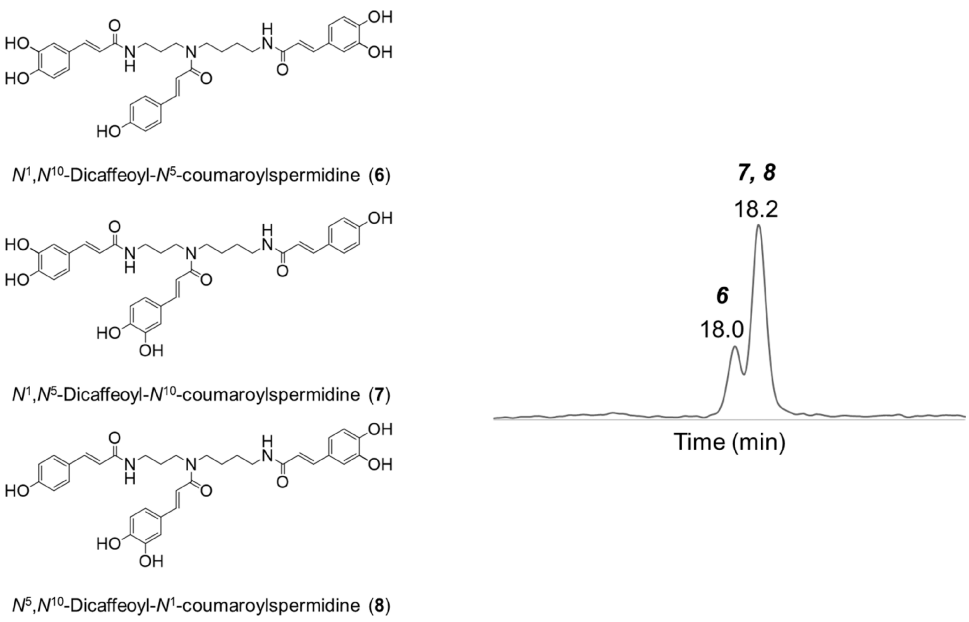

Figure 6. LC-MS analysis (extracted ion chromatogram for m/z 614) of the dicaffeoylcoumarylspermidine standard prepared using a one-pot synthesis by mixing spermidine with coumaric acid (∼1 equiv) and caffeic acid (∼2 equiv): three positional isomers are expected. The LC signal assignment (6−7−8) is proposed using LC-MS/MS analysis.

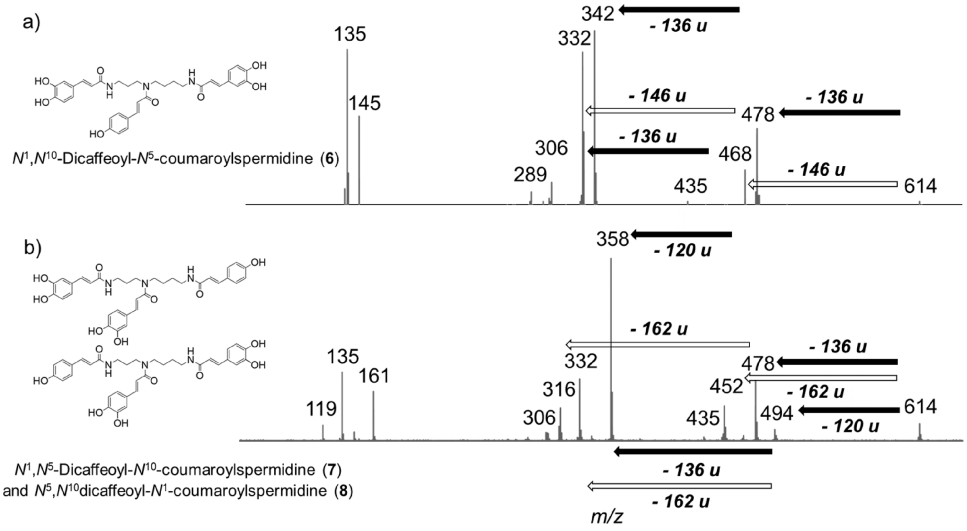

Figure 7. LC-MS/MS analysis of the dicaffeoylcoumarylspermidine standards prepared using a one-pot synthesis by mixing spermidine with coumaric acid (∼1 equiv) and caffeic acid (∼2 equiv). CID mass spectra of m/z 614 $[M - H]^-$ ions corresponding to the positional isomers eluting after (a) 18 and (b) 18.2 min (Waters QToF API-US, ESI(−), CE = 30 eV). See the text for structure assignment. Black and white arrows respectively correspond to the imidate and phenolate pathways.

LC-MS/MS experiments were performed, and the corresponding recorded CID mass spectra are compared in Figure 7. The presence of the coumaroyl residue is confirmed by the observation of the [m/z 119/120 u loss] and [m/z 145/146 u loss] pairs, whereas the caffeoyl groups are characterized by the [m/z 135/136 u loss] and [m/z 161/162 u loss] pairs. In particular, the specific detection of the m/z 468 (146 u loss) and m/z 145 fragment ions in Figure 7a allows one to attribute this CID spectrum to the N^1,N^{10}-dicaffeoyl-N^5-coumaroylspermidine isomer **6**. For compounds **7** and/or **8**, the presence of a caffeoyl residue in N^5 is confirmed by the observation of m/z 161 and m/z 452 (162 u loss) fragment ions in Figure 7b. Also, no transamidation reactions have been observed upon CID experiments in the negative ionization mode, allowing us to reliably distinguish N^1 and N^{10} substituents from N^5 substituents. Nevertheless, the CID spectral analysis did not allow a clear distinction between (**7**) and (**8**), because no characteristic fragments of N^1 or N^{10} positions were produced.

Based on the above developed mechanistic study, we identified several fragment ions that are signature ions for the structural characterization of phenolamides from natural extracts under ESI(−). Table 1 gathers relevant information that could be helpful for future phenolamide studies. From the $[M - H]^-$ precursor ions, the fragment ions generated by the two competitive dissociation routes, i.e., the phenolate and imidate pathways, are presented for all of the studied hydroxycinnamic acid moieties. We demonstrated that the imidate pathway is regiospecific at the extremities and is not

https://doi.org/10.1021/acs.jnatprod.3c00047
J. Nat. Prod. XXXX, XXX, XXX−XXX

Table 1. CID Analysis of Deprotonated Phenolamide Ions: Key-Fragment Ions

	phenolate pathway	imidate pathway	methyl cation transfer
hydroxycinnamic moiety	neutral loss (u)/corresponding ion		
p-Coumaroyl	−146/*m*/*z* 145	−120/*m*/*z* 119	/
Caffeoyl	−162/*m*/*z* 161	−136/*m*/*z* 135	/
Feruloyl	−176/*m*/*z* 175	−150/*m*/*z* 149	−136/*m*/*z* 135

occurring at the central position (tertiary amide). We also showed that the phenolate pathway is largely dominant at the central position but may occur at the extremities. Finally, even if no transamidation process has been detected, methyl cation migration between side-chains when methoxylated residues are present may affect the distinction between regioisomers.

CONCLUSIONS

Phenolamides are abundant phenylpropanoid metabolites found in nature and consist of hydroxycinnamic acids mono- or polyconjugated with polyamines, such as spermidine or spermine. Their important biotic and abiotic roles, notably in flower development, senescence, oxidative stress resilience, and pathogen protection, are documented. They are also abundantly present in pollens in which they are suggested to participate in several processes, such as pollen−stigma recognition or pollen adhesion to pollinators. However, their roles in plant−pollinator interactions are still poorly understood.

Facing the large diversity of natural phenolamides, based on the occurrence of different amine backbones and different hydroxycinnamic acid residues, the presence of positional isomers and stereoisomers due to the *cis*/*trans* isomerism of the C═C bonds, mass spectrometry hyphenated to liquid chromatography represents the most convenient analytical method for phenolamide analysis from natural extracts. Also, LC-MS/MS analysis, i.e., based on collision-induced dissociation (CID) experiments, may be efficient in phenolamide structural characterization, provided the dissociation reactions undergone by collision-activated ions are understood.

We here explored the CID processes undergone by the $[M - H]^-$ ions of spermidine-based phenolamides as model compounds for the phenolamide family. We proposed that two competitive dissociation routes, namely, the phenolate and imidate pathways, are in operation to account for the detected fragment ions. Interestingly, whereas the phenolate pathway is regioselective on the central amide of spermidine, the imidate pathway, requiring a deprotonated amide, may only occur at the extremities.

As far as the structural characterization of phenolamides is concerned, the present investigation confirms that LC-MS/MS experiments are very efficient in identifying the hydroxycinnamic residues and their positions but must be used with great care. Indeed, the MS/MS data generated on the $[M + H]^+$ ions, say in the positive ionization mode, are efficient to identify the hydroxycinnamic residues present on the polyamine backbone. This is also the case in the negative ionization mode, except that the inter-residue methyl migration involving feruloyl, hydroxyferuloyl, and sinapoyl residues may affect the residue identification by converting a feruloyl residue into a caffeoyl residue, for instance. However, since any LC-MS/MS experiment is preceded by an LC-MS analysis, the ambiguity raised by the methyl migration is often overcome by the phenolamide ion (accurate) mass measurement. On the other hand, as far as the regioisomer distinction is concerned, the fact that the transamidation reaction at play for the $[M + H]^+$ ions is not detected for the negatively charged ions, is clearly an advantage of the negative mode over the positive one. Note finally that in the negative ionization mode, the regiospecificity of the phenolate pathway at the internal (central) position(s) and of the imidate pathway at both extremities of the polyamide backbone allows discriminating the terminal positions from the internal one(s), but no discrimination between the terminal positions is achievable.

These observations may contribute to the distinction between phenolamide regioisomers and globally to the identification of phenolamides in natural extracts.

EXPERIMENTAL SECTION

Solvents. All solvents used were obtained from VWR. HPLC grade formic acid was purchased from ChemLab. Technical grade MeOH and CH_2Cl_2 were used for extraction, and HPLC-grade MeOH and formic acid were used for MS analysis. Milli-Q H_2O was produced by a PureLab Flex MANU38981 generator (Elga labwater).

Phenolamide Synthesis. Dicyclohexylcarbodiimide (DCC), spermidine, putrescine, *N*-methyl-1,3-diaminopropane, cadaverine, and *trans*-*p*-coumaric acid were purchased from Fisher Scientific. *trans*-Ferulic acid was provided by Sigma-Aldrich, *trans*-caffeic acid was provided by Apollo Scientific, and *trans*-cinnamic acid was provided by Janssen Chimica.

Each standard phenolamide was synthesized separately. Briefly, 10 mL of a solution of DCC (250 mM) in CH_2Cl_2 was added to 40 mL of a solution of the selected amine (18.5 mM) and hydroxycinnamic acid. For diamine-derived phenolamide, the ferulic or cinnamic acid concentration was 42.0 mM. For spermidine-derived phenolamides, the hydroxycinnamic acid concentration was 62.5 mM, and, in the case of dicaffeoylcoumaroylspermidine, the concentrations of caffeic and coumaric acids were 42.0 mM and 23.0 mM, respectively. The

Table 2. Accurate Mass Measurements of $[M + H]^+$ Ions Generated from the Synthesized Standard Phenolamides under ESI(+)

name	elemental composition	$[M + H]^+$ m/z_{calc}	$[M + H]^+$ m/z_{obs}	mass error (ppm)
N^1,N^5,N^{10}-Tri-*p*-coumaroylspermidine (**1**)	$C_{34}H_{38}N_3O_6^+$	584.2761	584.2733	4.8
N^1,N^7-Dicinnamoylcadaverine (**2**)	$C_{23}H_{27}N_2O_2^+$	363.2073	363.2089	4.4
N^1,N^5,N^{10}-Triferuloylspermidine (**3**)	$C_{37}H_{44}N_3O_9^+$	674.3078	674.3069	1.3
N^1,N^6-Diferuloylputrescine (**4**)	$C_{24}H_{29}N_2O_6^+$	441.2026	441.2018	1.8
N^1,N^5-Diferuloyl-N^1-methyl-propanediamine (**5**)	$C_{24}H_{29}N_2O_6^+$	441.2026	441.2012	3.2
N^1,N^{10}-Dicaffeoyl-N^5- coumaroylspermidine (**6**)	$C_{34}H_{38}N_3O_8^+$	616.2659	616.2628	5.0
N^1,N^5-Dicaffeoyl-N^{10}-coumaroylspermidine (**7**)	$C_{34}H_{38}N_3O_8^+$	616.2659	616.2628	5.0
N^5,N^{10}-Dicaffeoyl-N^1- coumaroylspermidine (**8**)	$C_{34}H_{38}N_3O_8^+$	616.2659	616.2628	5.0

https://doi.org/10.1021/acs.jnatprod.3c00047
J. Nat. Prod. XXXX, XXX, XXX−XXX

mixtures were stirred at room temperature overnight. Then, they were filtered on a Büchner funnel to remove the solid dicyclohexylurea (DCU) and CH_2Cl_2 was evaporated. The resulting yellowish solids were diluted in MeOH and characterized by LC-HRMS in positive ionization mode ($[M + H]^+$) (Table 2).

Mass Spectrometry Analysis. LC-MS and LC-MS/MS analyses were carried out using a Waters QToF API-US mass spectrometer (electrospray ion source) coupled to a Waters Alliance 2695 HPLC system. The column was a reversed-phase Phenomenex Kinetex C18 EVO column (150 × 2.1 mm inner diameter, 100 Å particle size). A binary gradient was performed at a flow rate of 0.25 mL/min. The mobile phase consisted of H_2O + 0.01% formic acid (solvent A) and MeOH (solvent B). The gradient program was as follows: A = 90%, B = 10% at t = 0 min; A = 70%, B = 30% at t = 6 min; A = 65%, B = 35% at t = 11 min; A = 50%, B = 50% at t = 18 min; A = 10%, B = 90% at t = 23 min; A = 0%, B = 100% at t = 25 min; A = 0%, B = 100% at t = 27 min; A = 90%, B = 10% at t = 30 min. Column temperature was 40 °C.

Typical ESI(+) and ESI(−) conditions were capillary voltage, 3.1 kV; cone voltage, 30 V; source temperature, 120 °C; desolvation temperature, 300 °C. Dry nitrogen was used as the ESI gas with a flow rate of 50 L/h for the gas cone and 500 L/h for the desolvation gas. For LC-MS analysis, the quadrupole was set to pass ions from m/z 50 to 1000, and all ions were transmitted into the pusher region of the time-of-flight analyzer for mass analysis with a 1 s integration time (fwhm 7000 at m/z 500). Data were acquired in continuum mode until acceptable average data were obtained (typically 20 scans). Accurate mass measurements (LC-HRMS in Table 2) were performed in the ESI(+) mode on the $[M + H]^+$ ions at a fwhm resolution of 8000 and using a coinjected standard molecule as the lock mass.

For the LC-MS/MS experiments, the ions of interest were mass-selected by a quadrupole mass filter. The selected ions were then submitted to collision against argon in the rf-only hexapole collision cell (pressure estimated at 0.9−1 mbar). The laboratory frame kinetic energy (collison energy - CE) was selected to afford intense enough fragment ion signals (see spectra). Fragment ions, as well as the nondissociated precursor ions, were finally mass-measured with the orthogonal axis ToF analyzer. Data are acquired in continuum mode until acceptable averaged data are obtained. The pseudo-MS^3 experiments presented in Figure 2 were performed as follows: the $[M-H]^-$ ions of tricoumaroylspermidine (**1**) (m/z 582) were generated under ESI(−) conditions. By increasing the cone voltage (CV) to 90 V, in-source CID processes were induced, allowing the production of the m/z 462 (imidate pathway) and 436 (phenolate pathway) fragment ions. These fragment ions were then mass-selected by the quadrupole analyzer and subjected to collisions against argon in the hexapolar collision cell (for the CE, see the figure captions). Fragment ions, as well as the nondissociated precursor ions, were finally mass-measured with the orthogonal axis ToF analyzer.

Theoretical Calculations. The geometries of all the molecules have been fully optimized in their neutral or anionic states at the MP2/6-31G** level using the Gaussian 16 package,[26] and minima have been confirmed through a vibrational mode analysis. All the reported simulated fragmentation energies correspond to the thermal enthalpy (estimated at 298.15 K) differences between the sum of the isolated products and reactants.

AUTHOR INFORMATION

Corresponding Author

Pascal Gerbaux − *Organic Synthesis and Mass Spectrometry Laboratory (S^2MOs), Research Institute for Biosciences, University of Mons - UMONS, B-7000 Mons, Belgium;* orcid.org/0000-0001-5114-4352; Email: pascal.gerbaux@umons.ac.be

Authors

Irène Semay − *Organic Synthesis and Mass Spectrometry Laboratory (S^2MOs), Research Institute for Biosciences, University of Mons - UMONS, B-7000 Mons, Belgium;* orcid.org/0000-0002-4197-0316

Vincent Lemaur − *Laboratory for Chemistry of Novel Materials, Materials Research Institute, University of Mons - UMONS, Mons B-7000, Belgium;* orcid.org/0000-0001-8601-286X

Antoine Gekière − *Laboratory of Zoology, Research Institute for Biosciences, University of Mons - UMONS, B-7000 Mons, Belgium;* orcid.org/0000-0001-5337-1305

Maryse Vanderplanck − *Laboratory of Zoology, Research Institute for Biosciences, University of Mons - UMONS, B-7000 Mons, Belgium; CEFE, University of Montpellier, CNRS, EPHE, IRD, 34090 Montpellier, France*

Pierre Duez − *Unit of Therapeutic Chemistry and Pharmacognosy, Faculty of Medicine and Pharmacy, University of Mons - UMONS, B-7000 Mons, Belgium*

Denis Michez − *Laboratory of Zoology, Research Institute for Biosciences, University of Mons - UMONS, B-7000 Mons, Belgium*

Complete contact information is available at: https://pubs.acs.org/10.1021/acs.jnatprod.3c00047

Notes

The authors declare no competing financial interest.

ACKNOWLEDGMENTS

This work was a part of the ARC 'Actions de Recherche Concertées' project 'METAFLORE, 2019−2023'. The PhD grant of I.S. is supported by the ARC project METAFLORE. A.G. is supported by a F.R.S.-FNRS PhD grant "Aspirant".

REFERENCES

(1) Kyselka, J.; Bleha, R.; Dragoun, M.; Bialasova, K.; Horackova, S.; Schatz, M.; Slukova, M.; Filip, V.; Synytsya, A. *J. Agric. Food Chem.* **2018**, *66* (42), 11018−11026.

(2) Jiang, J. S.; Lu, L.; Yang, Y. J.; Zhang, J. L.; Zhang, P. C. *J. Asian Nat. Prod. Res.* **2008**, *10* (5), 447−451.

(3) Park, S. B.; Song, K.; Kim, Y. S. *Planta Medica Int. Open* **2017**, *4*, e43−e51.

(4) Werner, C.; Hu, W.; Lorenzi-Riatsch, A.; Hesse, M. *Phytochemistry* **1995**, *40* (2), 461−465.

(5) Bento-Silva, A.; Duarte, N.; Mecha, E.; Belo, M.; Vaz Patto, M. C.; do Rosário Bronze, M. *Foods* **2020**, *9* (10), 1471.

(6) Handrick, V.; Vogt, T.; Frolov, A. *Anal. Bioanal. Chem.* **2010**, *398*, 2789−2801.

(7) Gaquerel, E.; Heiling, S.; Schoettner, M.; Zurek, G.; Baldwin, I. T. *J. Agric. Food Chem.* **2010**, *58* (17), 9418−9427.

(8) Youhnovski, N.; Bigler, L.; Werner, C.; Hesse, M. *Helv. Chim. Acta* **1998**, *81* (9), 1654−1671.

(9) Strack, D.; Eilert, U.; Wray, V.; Wolff, J.; Jaggy, H. *Phytochemistry* **1990**, *29* (9), 2893−2896.

(10) Macoy, D. M.; Kim, W. Y.; Lee, S. Y.; Kim, M. G. *Plant Biotechnol. Rep.* **2015**, *9* (5), 269−278.

(11) Roumani, M.; Besseau, S.; Gagneul, D.; Robin, C.; Larbat, R. *J. Exp. Bot.* **2021**, *72* (7), 2334−2355.

(12) Vogt, T. *J. Exp. Bot.* **2018**, *69* (22), 5311−5318.

(13) Roumani, M.; Duval, R. E.; Ropars, A.; Risler, A.; Robin, C.; Larbat, R. *Biomed. Pharmacother.* **2020**, *131* (November 2020), 110762.

(14) Hu, W.; Werner, C.; Hesse, M. *Helv. Chim. Acta* **1998**, *81*, 342−352.

(15) Li, Z.; Zhao, C.; Zhao, X.; Xia, Y.; Sun, X.; Xie, W.; Ye, Y.; Lu, X.; Xu, G. *Anal. Chem.* **2018**, *90* (24), 14321−14330.

(16) Fellenberg, C.; Böttcher, C.; Vogt, T. *Phytochemistry* **2009**, *70* (11−12), 1392−1400.

https://doi.org/10.1021/acs.jnatprod.3c00047
J. Nat. Prod. XXXX, XXX, XXX−XXX

(17) Gaquerel, E.; Kotkar, H.; Onkokesung, N.; Galis, I.; Baldwin, I. T. *PLoS One* **2013**, *8* (5), e62336.
(18) Zhao, G.; Qin, G. W.; Gai, Y.; Guo, L. H. *Chem. Pharm. Bull.* **2010**, *58* (7), 950−952.
(19) Bigler, L.; Schnider, C. F.; Hu, W.; Hesse, M. *Helv. Chim. Acta* **1996**, *79*, 2152−2163.
(20) Bigler, L.; Hesse, M. *J. Am. Soc. Mass Spectrom.* **1995**, *6*, 634−637.
(21) Hu, W.; Reder, E.; Hesse, M. *Helv. Chim. Acta* **1996**, *79*, 2137−2151.
(22) Cheng, C.; Gross, M. L. *Mass Spectrom. Rev.* **2000**, *19* (6), 398−420.
(23) Afonso, C.; Cole, R. B.; Tabet, J.-C. Dissociation of Even-Electron Ions. In *Electrospray and MALDI Mass Spectrometry: Fundamentals, Instrumentation, Practicalities, and Biological Applications*; Cole, R. B., Ed.; John Wiley & Sons, Inc: Hoboken, 2010; pp 631−682.
(24) Paizs, B.; Suhai, S. *Mass Spectrom. Rev.* **2005**, *24* (4), 508−548.
(25) de Hoffmann, E.; Stroobant, V. *Spectrométrie de Masse*, 3rd ed.; Dunod: Paris, 2005.
(26) Frisch, M. J.; Trucks, G. W.; Schlegel, H. B.; Scuseria, G. E.; Robb, M. A.; Cheeseman, J. R.; Scalmani, G.; Barone, V.; Petersson, G. A.; Nakatsuji, H.; Li, X.; Caricato, M.; Marenich, A. V.; Bloino, J.; Janesko, B. G.; Gomperts, R.; Mennucci, B.; Hratchian, H. P.; Ortiz, J. V.; Izmaylov, A. F.; Sonnenberg, J. L.; Williams-Young, D.; Ding, F.; Lipparini, F.; Egidi, F.; Goings, J.; Peng, B.; Petrone, A.; Henderson, T.; Ranasinghe, D.; Zakrzewski, V. G.; Gao, J.; Rega, N.; Zheng, G.; Liang, W.; Hada, M.; Ehara, M.; Toyota, K.; Fukuda, R.; Hasegawa, J.; Ishida, M.; Nakajima, T.; Honda, Y.; Kitao, O.; Nakai, H.; Vreven, T.; Throssell, K.; Montgomery, J. A., Jr.; Peralt, J. E.; Ogliaro, F.; Bearpark, M. J.; Heyd, J. J.; Brothers, E. N.; Kudin, K. N.; Staroverov, V. N.; Keith, T. A.; Kobayashi, R.; Normand, J.; Raghavachari, K.; Rendell, A. P.; Burant, J. C.; Iyengar, S. S.; Tomasi, J.; Cossi, M.; Millam, J. M.; Klene, M.; Adamo, C.; Cammi, R.; Ochterski, J. W.; Martin, R. L.; Morokuma, K.; Farkas, O.; Foresman, J. B.; Fox, D. J. *Gaussian 16, Revision A.03*. Gaussian, Inc.: Wallingford CT, 2016.

https://doi.org/10.1021/acs.jnatprod.3c00047
J. Nat. Prod. XXXX, XXX, XXX−XXX